Photoneutron Cross Sections for Sn^{116}, Sn^{117}, Sn^{118}, Sn^{119}, Sn^{120}, Sn^{124}, and Indium†

S. C. Fultz, B. L. Berman, J. T. Caldwell, R. L. Bramblett,* and M. A. Kelly‡
Lawrence Radiation Laboratory, University of California, Livermore, California 94550

(Received 17 March 1969)

Monochromatic photons obtained from the annihilation in flight of fast positrons were used to measure photoneutron cross sections for a number of tin isotopes and indium. Total cross sections for Sn^{116}, Sn^{117}, Sn^{118}, Sn^{119}, Sn^{120}, Sn^{124}, and In have peak values of 266, 254, 255, 253, 280, 283, and 266 mb at energies of 15.67, 15.66, 15.60, 15.54, 15.40, 15.18, and 15.63 MeV, respectively. The respective integrated cross sections were found to be 1.67, 1.89, 1.85, 2.00, 2.07, 2.01, and 1.88 MeV b; while the respective $(\gamma, 2n)$ integrated cross sections were 0.414, 0.475, 0.531, 0.598, 0.673, 0.670, and 0.509 MeV b. Single-nucleon effects on the giant resonance were examined, and shell effects have been determined. Other nuclear quantities determined include nuclear level densities, pairing energies, and integrated moments.

I. INTRODUCTION

THE tin isotopes and indium comprise a series of nuclides differing from each other in most cases by only one nucleon. They therefore make possible a study of single-nucleon effects on parameters which are significant to the nuclear photo effect for the region in the middle of the Periodic Table. With such a study in mind, the measurements described in this report were undertaken. No systematic study of these isotopes has been undertaken previously, although considerable work has been reported on selected members of this series. A brief review of some of the earlier work is given below.

Fuller *et al.*[1] measured the photoneutron yield cross section of natural tin with the use of bremsstrahlung radiation, while Hartley *et al.*[2] used the $Li(p, \gamma)$ γ rays for such measurements. Allum *et al.*[3] measured the angular distribution of fast photoneutrons coming from the (γ, n) reaction on natural tin, and Tohei *et al.*[4] examined the (γ, n) cross section of tin relative to that of lead. Kuo *et al.*[5] measured the (γ, n) yield for Sn^{112} and Sn^{124} relative to the $Cu^{63}(\gamma, n)Cu^{62}$ reaction, using bremsstrahlung, and obtained measurements on the cross sections[6] for the reactions $Sn^{120}(\gamma, p)In^{119}$ and $Sn^{120}(\gamma, pn)In^{118}$. The results obtained by these experimenters are summarized in Table I.

For the case of indium, a considerable number of measurements have been made, a few of which are described below. Anashking[7] examined the angular and energy distribution of photoneutrons from In^{115} using photographic plates with Ilford G-5 emulsions. Bogdankevich *et al.*[8] measured the yield cross section $\sigma[(\gamma, n)+2(\gamma, 2n)+3(\gamma, 3n)]$ for In^{115} and for the 40-day half-life In^{115m}. Hurst and Donahue[9] used monochromatic capture γ rays to measure the photoneutron yield cross section of In at 9.72 and 10.83 MeV. Mitchell and McNeill[10] examined the angular distributions of photoprotons, while Dixon[11] measured the angular distribution of photoneutrons from In. The results obtained for In from previous experiments, which are significant to the present report, are summarized in Table I.[12]

II. APPARATUS AND METHOD

The present measurements were made using monochromatic photons obtained from the annihilation in flight of fast positrons.[13–15] The neutrons were detected in a 4π paraffin-moderated neutron detector containing 48 BF_3 chambers filled to a pressure of 1670 Torr with enriched $B^{10}F_3$. The efficiency of the detector was approximately 0.40. The neutron counts were separated so that single, double, triple, etc., counts per beam burst were counted on separate scaling circuits. From these data, the partial cross sections $\sigma(\gamma, n)$, $\sigma(\gamma, 2n)$, and $\sigma(\gamma, 3n)$ were calculated using a computer code. The efficiency of the neutron detector was monitored by use of the "ring-ratio" method.[15] Corrections for the

† Work performed under the auspices of the U.S. Atomic Energy Commission.

* Present address: Gulf General Atomic Inc., San Diego, Calif. 92112.

‡ Present address: Hewlett-Packard Corp., Palo Alto, Calif. 94304.

[1] E. G. Fuller, B. Petree, and M. S. Weiss, Phys. Rev. **112**, 554 (1958).

[2] W. H. Hartley, W. E. Stephens, and E. J. Winhold, Phys. Rev. **104**, 178 (1956).

[3] F. R. Allum, T. W. Quirk, and B. M. Spicer, Nucl. Phys. **53**, 545 (1964).

[4] T. Tohei, M. Sugawara, S. Mori, and M. Kimura, J. Phys. Soc. Japan **16** (1961).

[5] Kuo Ch'i-Ti, B. S. Ratner, and B. V. Sergeev, Zh. Eksperim. i Teor. Fiz. **40**, 85 (1961) [English transl.: Soviet Phys.—JETP **13**, 60 (1961)].

[6] Kuo Ch'i-Ti and B. S. Ratner, Zh. Eksperim i Teor. Fiz. **39**, 1578 (1960) [English transl.: Soviet Phys.—JETP **12**, 1098 (1961)].

[7] E. S. Anashking, Zh. Eksperim. i Teor. Fiz. **43**, 1197 (1962) [English transl.: Soviet Phys.—JETP **16**, 847 (1963)].

[8] O. V. Bogdankevich, L. E. Lazareva, F. A. Nikolaev, Zh. Eksperim i Teor. Fiz., **31**, 405 (1956) [English transl.: Soviet Phys.—JETP **4**, 320 (1957)].

[9] R. R. Hurst and D. J. Donahue, Nucl. Phys. **A91**, 365 (1967).

[10] O. M. M. Mitchell and K. G. McNeill, Can. J. Phys. **41**, 871 (1963).

[11] W. R. Dixon, Can. J. Phys. **33**, 785 (1955).

[12] O. V. Bogdankevich, B. I. Goryachev, and V. A. Zapevalov, Zh. Eksperim. i Teor. Fiz. **42**, 1502 (1962) [English transl.: Soviet Phys.—JETP **15**, 1044 (1962)].

[13] S. C. Fultz, R. L. Bramblett, J. T. Caldwell, and N. A. Kerr, Phys. Rev. **127**, 1273 (1962).

[14] S. C. Fultz, R. L. Bramblett, J. T. Caldwell, N. E. Hansen, and C. P. Jupiter, Phys. Rev. **128**, 2345 (1962).

[15] B. L. Berman, J. T. Caldwell, R. R. Harvey, M. A. Kelly, R. L. Bramblett, and S. C. Fultz, Phys. Rev. **162**, 1098 (1967).

TABLE I. Previous results on tin isotopes and indium.

Nucleus	Reaction	σ_{max} (mb)	E_{max} (MeV)	Γ (MeV)	$\int\sigma dE$ (MeV mb)	Photon source	Ref.
Nat Sn	(γ, n)	300		5.0	1860	30-MeV bremss.	1
Sn	(γ, n)	195				Li(p, γ)	
Sn	(γ, n)				1830	30-MeV bremss.	4
Sn^{112}	(γ, n)	340±40	16.0	5.0	1820±100	30-MeV bremss.	5
Sn^{124}	(γ, n)	300±30	15.5	5.0	1560±80	30-MeV bremss.	5
Sn^{120}	(γ, p)	6.5±0.6	20.0	3.5±0.5	5.0±0.1	30-MeV bremss.	6
Sn^{120}	(γ, pn)	1.9	24.5	2.5	28.0±3.0	30-MeV bremss.	6
In^{115}	(γ, n)	166	14.00	3.0	780	30-MeV bremss.	12
		240	16.25	3.8	1430	30-MeV bremss.	12
In^{115}	(γ, n)	280±29	15.1	5.0	1800	27-MeV bremss.	8
In^{115}	(γ, n)	17.1±2.6				9.72 MeV	9
		33.3±2.7				10.83 MeV	9

neutron detector efficiency as a function of photon excitation energy then were applied to the data, since the average photoneutron energy changes with energy of the incident photons.

The photons were measured with a transmission ion chamber filled with Xe to a pressure of $\frac{1}{2}$atm. The photon energy resolution varied from approximately 300 keV at 10 MeV to 400 keV at 30 MeV. The absolute cross section was determined with an accuracy of approximately 7%. This includes uncertainty in the single photoneutron cross sections attributable to a 4% uncertainty in correcting the data for those neutrons produced by the bremsstrahlung photons in the incident beam.

The enriched isotopic samples consisted of pure metal, mainly in the shape of disks of 1.5 in. diam. They were inserted at the center of an axial hole in the neutron detector and were mounted in a cylindrical styrofoam container of low mass. Characteristics of the samples are given in Table II. A list of theshold energies[16] for the reactions of interest in the present experiment is given in Table III.

The direct measurement of the higher-multiplicity cross sections in the present work makes possible unambiguous evaluation of the integrated cross sections and of features in the shape of the giant resonance. Much of the earlier data is of limited value because of the lack of this information. Such measurements also reveal the more subtle single-nucleon effects on the characteristics of the giant resonance, such as its width and the ratio of the integrated $\sigma(\gamma, 2n)$ to $\sigma(\gamma_{tot})$ cross sections, as will be shown subsequently in this report.

The absolute photon intensity was obtained by calibration of the ion chamber with an 8×8-in. NaI(Tl) detector. The calibration was performed by measuring simultaneously the response of the transmission ion chamber and the spectrum of the photons as determined by the NaI(Tl) spectrometer. In order to select only annihilation photons from the mixture with positron bremsstrahlung radiation, the response functions for the NaI(Tl) crystal were measured as a function of photon energy by application of the coincidence method to the two-photon annihilation process.

A. Ring-Ratio Data

The neutron detector consists of four concentric annular arrays of BF_3 tubes in a paraffin moderator. Counts from each array are recorded separately. Although the total detector efficiency is reasonably independent of neutron energy, the ratio of the efficiencies of the outside to the innermost rings is a sensitive measure of the average neutron energy. This ring ratio is shown in Figs. 1–7. The ring-ratio data for Sn^{116} are given in Fig. 1. They show a monotonically smooth rise as a function of photon energy, followed by a sharp drop

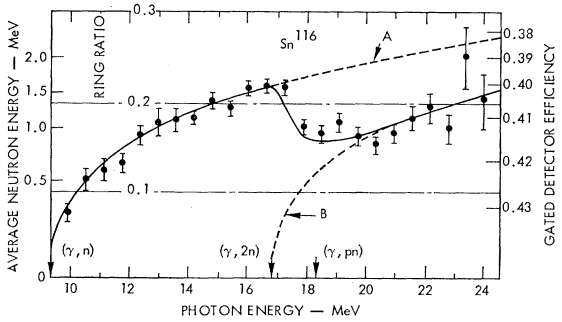

FIG. 1. Ring-ratio and efficiency data for Sn^{116}. The solid lines and extension are calculated curves based on Eq. (1).

[16] J. H. E. Mattauch, W. Thiele, and A. H. Wapstra, Nucl. Phys. **67**, 32 (1965).

TABLE II. Characteristics of samples used.

Dominant isotope	Sample weight (g)	Percent abundance (according to mass number) 112	113	114	115	116	117	118	119	120	122	124
Sn^{116}	50.02	<0.01	0.00	0.03	0.06	95.74	1.02	1.49	0.32	1.06	0.13	0.15
Sn^{117}	35.33	0.08	0.00	0.04	0.06	2.34	89.2	4.5	1.12	2.16	0.26	0.28
Sn^{118}	144.8	<0.03	0.00	<0.03	<0.03	0.39	0.4	97.15	0.64	1.20	0.10	0.12
Sn^{119}	54.85	<0.03	0.00	<0.03	<0.03	0.65	0.63	3.01	89.8	5.34	0.28	0.27
Sn^{120}	186.8	<0.05	0.00	<0.05	<0.05	0.20	0.12	0.5	0.39	98.39	0.15	0.26
Sn^{124}	45.8	<0.02	0.00	0.03	<0.03	0.99	0.54	1.75	0.64	2.49	0.75	92.8
Natural Sn	...	0.96	0.00	0.66	0.35	14.30	7.61	24.03	8.58	32.85	4.72	5.94
Indium	484.9	0.00	4.28	0.00	95.72	0.00	0.00	0.00	0.00	0.00	0.00	0.00

in the region of the $(\gamma, 2n)$ threshold, indicating a drop in the average neutron energy at this point. The solid curve through the data is the calculated ring ratio based on a neutron spectrum given by

$$N(E_n) \equiv \text{const}(E_n/U^2)\exp(2aU)^{1/2}, \quad (1)$$

where U is the excitation energy of the residual nucleus, and E_n is the neutron energy. Curve A of Fig. 1 is the calculated value for the ring ratio for (γ, n) neutrons only, while curve B applies to $(\gamma, 2n)$ neutrons. These calculations were based upon the level-density parameter (a) of 10 ± 2 MeV^{-1} for (γ, n) and $(\gamma, 2n)$ neutrons.

The ring-ratio data for Sn^{117} (Fig. 2) are characteristic of a constant average neutron energy (except near threshold where data are lacking). For Sn^{118} (Fig. 3) the ring ratio is again nearly constant but shows a rise in average neutron energy near the (γ, n) threshold. Sn^{119} and Sn^{120} (Figs. 4 and 5) show little change in average neutron energy over the range examined but have slight drops in average energy at the $(\gamma, 2n)$ threshold. The ring-ratio data for Sn^{124} (Fig. 6) are characteristic of a nearly constant neutron energy, but also indicate a drop in the average neutron energy just above the $(\gamma, 2n)$ threshold. In general, however, the ring-ratio data for all the tin isotopes examined indicate that the average neutron energy is nearly constant over a wide range of incident photon energies with a slight reduction in the average energy at the $(\gamma, 2n)$ thresholds.

The case for In^{115} is somewhat different. Here the average neutron energy follows a monotonically smooth, slowly rising curve, approaching an asymptotic limit at about 8 MeV above the (γ, n) threshold (Fig. 7). This contrasts with the ring-ratio data for the tin isotopes, in which the average neutron energy rises rapidly to a nearly constant value, just above the (γ, n) threshold. The slow rise indicates a large fraction of low-energy neutrons in the neutron spectrum. A factor which might influence the ring ratio is that the residual nucleus In^{114} is odd-odd and therefore the density of possible residual levels is especially high. There is also the possibility that a new reaction channel is opening up, causing a sharing of the excitation energy among a greater number of available levels. A similar behavior was observed for the ring-ratio data of Y^{89},[15] for which the residual nucleus Y^{88} is also an odd-odd nucleus.

TABLE III. Thresholds for tin isotopes[a] (MeV).

	(γ, n)	$(\gamma, 2n)$	$(\gamma, 3n)$	(γ, p)	(γ, pn)
Sn^{116}	9.563±0.007	17.100±0.010	27.42±0.03	9.270±0.009	18.30±0.02
Sn^{117}	6.941±0.005	16.505±0.008	24.04±0.02	9.486±0.024	16.21±0.05
Sn^{118}	9.331±0.005	16.272±0.003	25.84±0.01	10.016±0.010	18.82±0.04
Sn^{119}	6.481±0.005	15.812±0.003	22.75±0.01	9.900±0.400	16.50±0.80
Sn^{120}	9.110±0.004	15.591±0.003	24.92±0.01	10.820±0.120	19.01±0.54
Sn^{124}	8.506±0.011	14.437±0.003	23.23±0.01	7.070±0.012	20.30±0.80
In^{115}	9.034±0.010	16.346±0.011	25.77±0.01	8.740±0.009	15.86±0.01

[a] See Ref. 16.

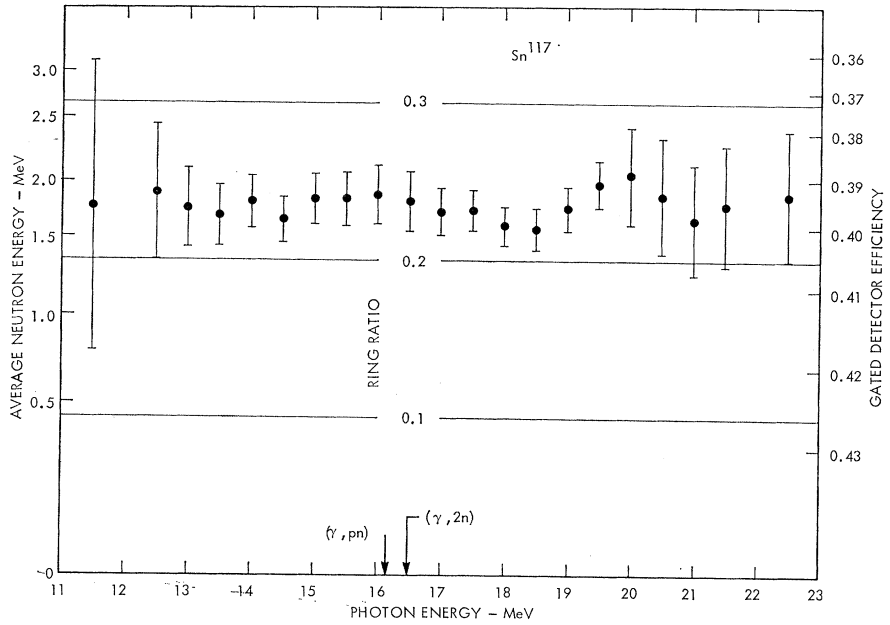

FIG. 2. Ring-ratio and efficiency data for Sn^{117}.

B. Cross-Section Data

The cross-section data for Sn^{116}, Sn^{117}, Sn^{118}, Sn^{119}, Sn^{120}, Sn^{124}, and In^{115} are presented in Figs. 8–14. Summaries of parameters deduced from these data are given in subsequent tables.

1. Sn^{116}. The photoneutron cross sections for Sn^{116} are shown in Figs. 8(a)–8(c). There appears to be a small amount of structure near the threshold and above the peak of the giant resonance. The singles cross section drops to zero a few MeV above the $(\gamma, 2n)$ threshold as is expected when higher multiplicity reactions take over the photon absorption process. The total cross section has a maximum of 272 mb at 15.3 MeV. The $(\gamma, 2n)$ cross section is shown in Fig. 8(b). It rises sharply to a peak value of 62 mb at 19.8 MeV. The $(\gamma, 2n)$ threshold appears at 17.0±0.1 MeV, in agreement with the value 17.1 MeV given by Mattauch *et al.*[16] The total photoneutron cross section is given in Fig. 8(c). It has been fitted with a Lorentz curve having parameters given in Table IV.

The width Γ of the giant resonance of Sn^{116} is 4.19 MeV, full width at half-maximum (FWHM), and is the narrowest for the group of isotopes examined in this experiment. Although Sn^{116} has 66 neutrons and does not have a closed neutron shell, the effect of adding valence neutrons is evident in the broadening of the giant resonance, as shown in Table IV.

2. Sn^{117}. The cross-section data for Sn^{117} are given in Figs. 9(a)–9(d). The total cross section rises to a maximum of 254 mb at 15.7 MeV and shows a slight amount of structure on the high-energy side of the giant resonance at approximately 22 MeV. The $(\gamma, 2n)$ cross section reaches a peak value of 71 mb at 18.9 MeV. The $(\gamma, 3n)$ cross section appears to be less than 10 mb from threshold (24.0 MeV) up to approximately 30 MeV, then rises slightly. The data can be fitted with a Lorentz line having the parameters given in Table IV.

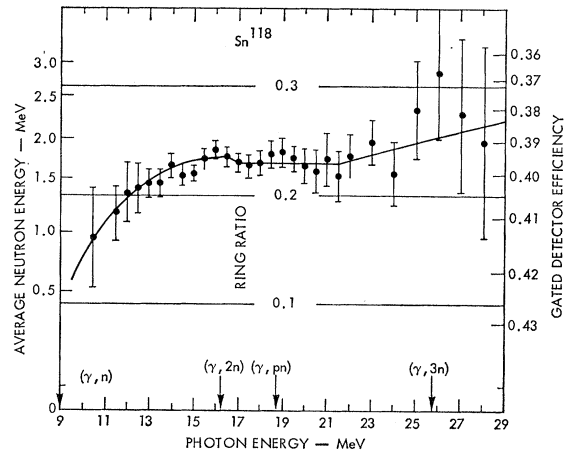

FIG. 3. Ring-ratio and efficiency data for Sn^{118}.

TABLE IV. Lorentz-curve parameters for giant-resonance data.

Nucleus	E_m (MeV)	σ_m (mb)	Γ (MeV)
Sn^{116}	15.67±0.04	266±7	4.19±0.06
Sn^{117}	15.66±0.04	254±7	5.02±0.06
Sn^{118}	15.60±0.04	255±7	4.76±0.06
Sn^{119}	15.54±0.04	253±7	4.81±0.06
Sn^{120}	15.40±0.04	280±8	4.88±0.06
Sn^{124}	15.18±0.04	283±8	4.81±0.06
In^{115}	15.63±0.04	266±7	5.24±0.06

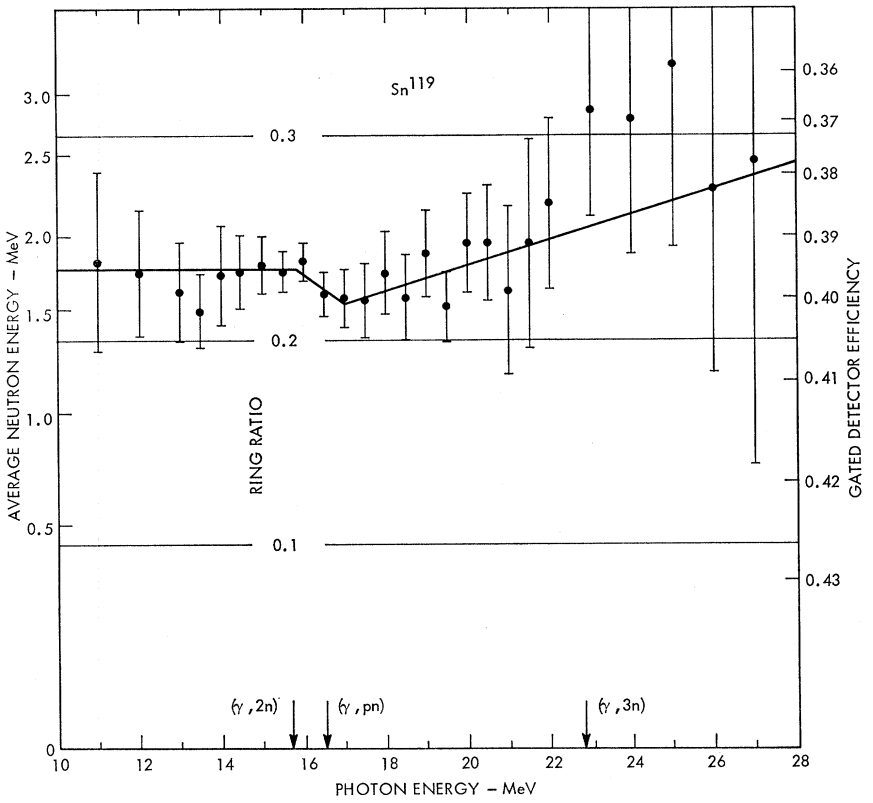

FIG. 4. Ring-ratio and efficiency data for Sn^{119}.

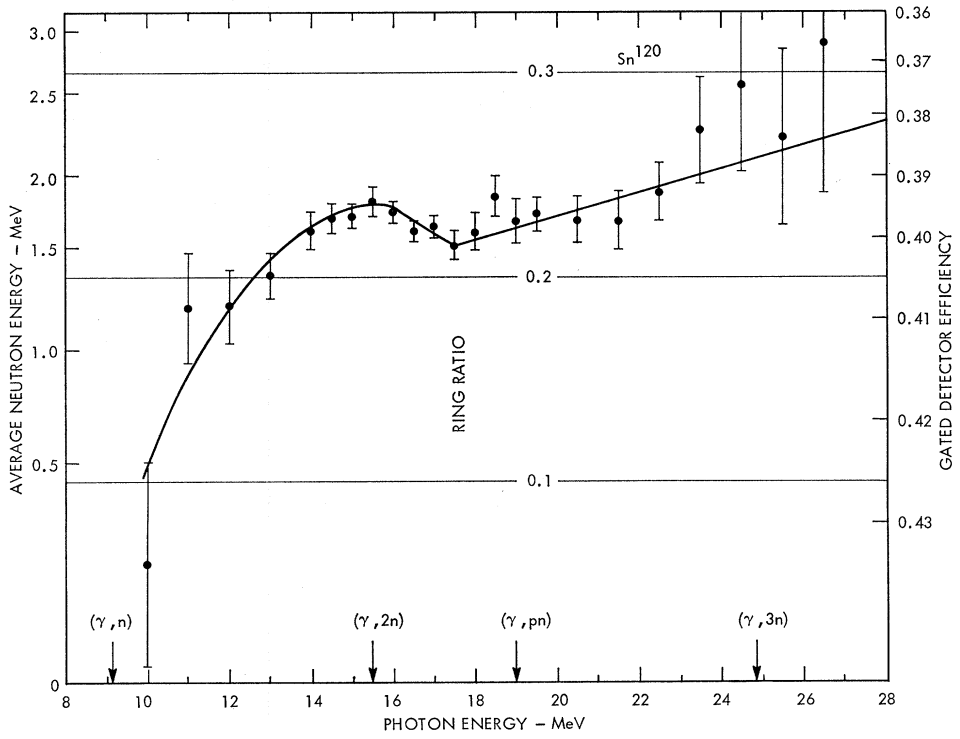

FIG. 5. Ring-ratio and efficiency data for Sn^{120}.

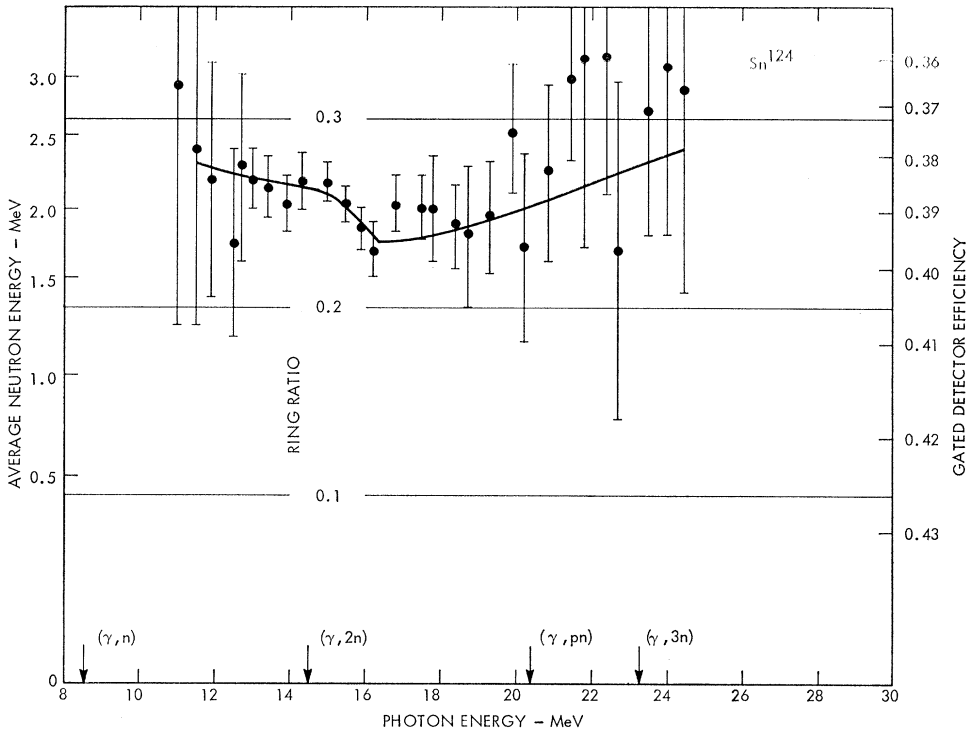

FIG. 6. Ring-ratio and efficiency data for Sn^{124}.

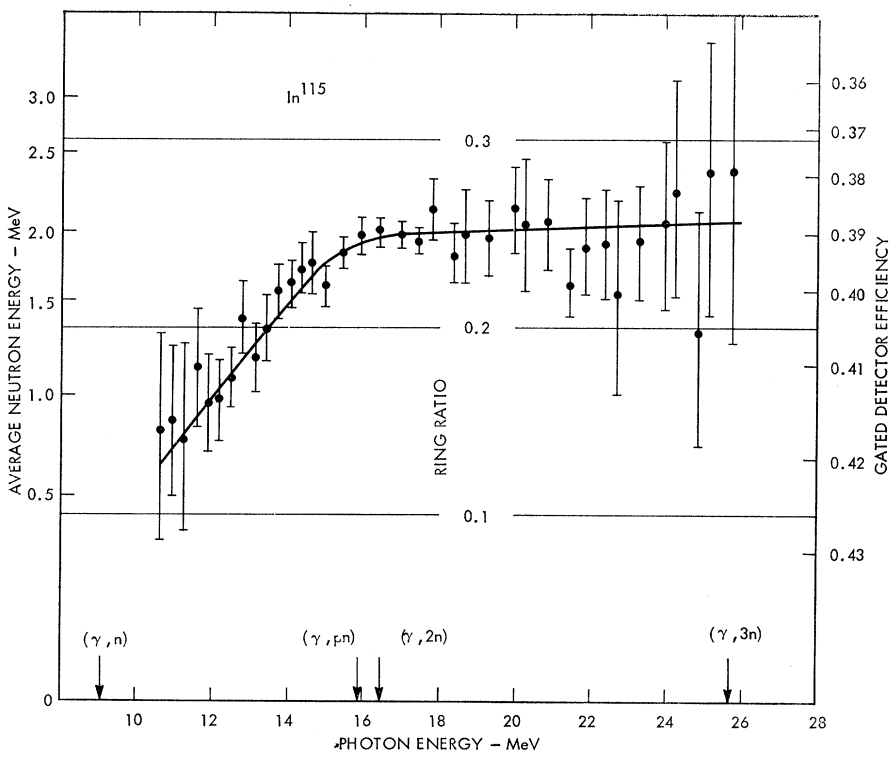

FIG. 7. Ring-ratio and efficiency data for In.

The major contaminant in the Sn^{117} sample was Sn^{118} (4.5%). This, however, would not be expected to appreciably alter the shape of either the $\sigma(\gamma, n)$ or the $\sigma(\gamma, 2n)$ data curves, since the $(\gamma, 2n)$ thresholds are similar and the (γ, n) threshold of Sn^{118} is 2.3 MeV higher than that for Sn^{117}.

3. Sn^{118}. Figures 10(a)–10(d) give cross-section data for Sn^{118}. The total cross section rises to a maximum of 255 mb at 15.6 MeV. Some structure in the cross section appears on the high-energy side of the giant resonance (as in the case of Sn^{117}) at approximately 25 MeV. The $(\gamma, 2n)$ cross section rises to a maximum of 78 mb at 19.0 MeV. The $(\gamma, 3n)$ data are sparse, but indicate that the cross section is less than 10 mb in the energy range from threshold (25.8 MeV) to approximately 30 MeV.

4. Sn^{119}. The data for Sn^{119} are shown in Figs. 11(a)–11(d). The total photoneutron cross section reaches a maximum of 259 mb at 15.5 MeV. The $(\gamma, 2n)$ cross section rises to a maximum of 92 mb at 18.5 MeV. The main contaminant of the Sn^{119} sample was Sn^{120}. Since the latter has nearly the same $(\gamma, 2n)$ threshold and similar features of the giant resonance, it would not be expected to influence the photoneutron cross-section measurements for Sn^{119}. The $(\gamma, 3n)$ data are more abundant and show a greater cross section than those for Sn^{118}. The data rise to approximately 20 mb between threshold (22.75 MeV) and 30 MeV. The $(\gamma, 2n)$ cross section can be observed to decrease significantly to-

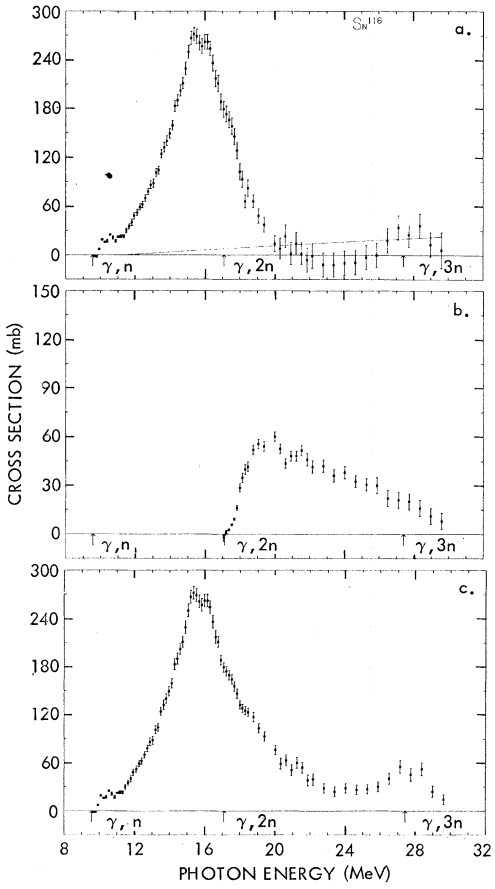

FIG. 8. (a) Single-photoneutron cross section $\sigma[(\gamma, n)+(\gamma, pn)]$ for γ rays incident on Sn^{116}. The thresholds are from Ref. 16. The dashed line represents the maximum increase in cross section which would be caused by a 4% uncertainty in the normalization constant. (b) The double-photoneutron cross section $\sigma[(\gamma, 2n)]$. (c) The total-photoneutron cross section $\sigma[(\gamma, n)+(\gamma, pn)+(\gamma, 2n)+(\gamma, 3n)]$. The latter can be fitted with a Lorentz line having the parameters given in Table IV.

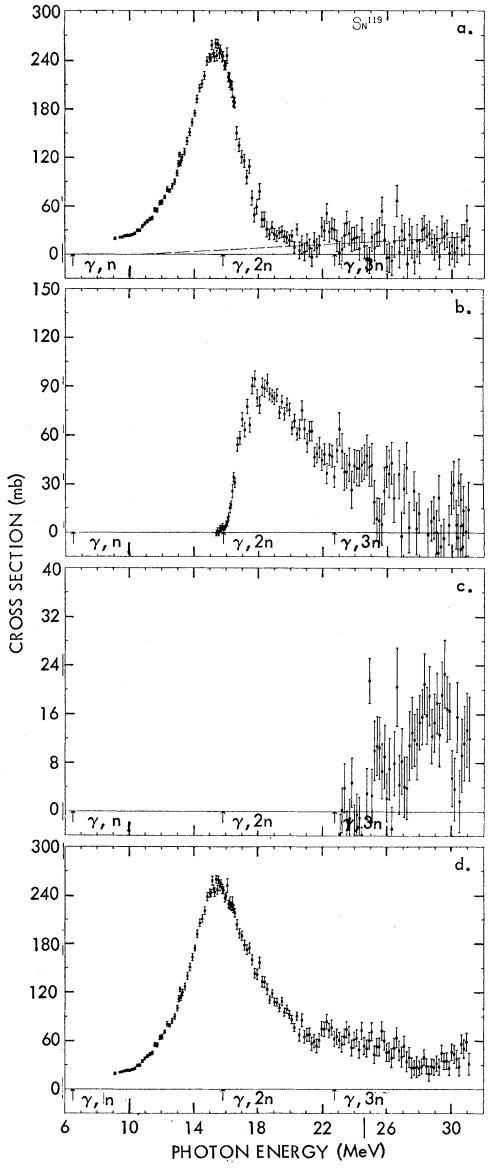

FIG. 9. (a) Single-photoneutron cross section $\sigma[(\gamma, n)+(\gamma, pn)]$ for γ rays incident on Sn^{117}. (b) The double-photoneutron cross section $\sigma(\gamma, 2n)$. (c) The triple-photoneutron cross section $\sigma(\gamma, 3n)$. (d) The total-photoneutron cross section $\sigma[(\gamma, n)+(\gamma, pn)+(\gamma, 2n)+(\gamma, 3n)]$ for Sn^{117}. The data of curve (d) can be fitted with a Lorentz line (up to 17 MeV) with parameters given in Table IV.

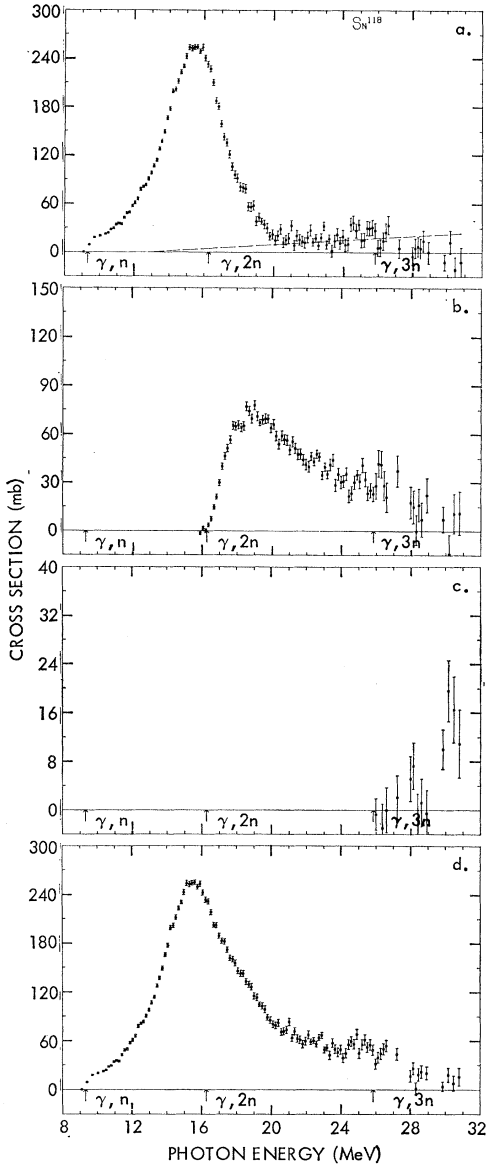

FIG. 10. (a) Single-photoneutron cross-section data $\sigma[(\gamma, n)+(\gamma, pn)]$ for γ rays incident on Sn^{118}. The dashed line represents the maximum increase in cross section which would be caused by a 4% uncertainty in the normalization constant. (b) Double-photoneutron cross-section data $\sigma(\gamma, 2n)$. (c) Triple-photoneutron cross-section data $\sigma(\gamma, 3n)$. (d) Total-photoneutron cross-section $\sigma[(\gamma, n)+(\gamma, pn)+(\gamma, 2n)+(\gamma, 3n)]$. The data of curve (d) can be fitted with a Lorentz line (up to 17.5 MeV) with parameters given in Table IV.

wards zero as the $(\gamma, 3n)$ process takes over, in keeping with statistical predictions.

5. Sn^{120}. Data for Sn^{120} are shown in Figs. 12(a)–12(d). Some structure appears in the cross section near threshold and on the high-energy side of the giant resonance, at approximately 23 MeV. The cross section reaches a maximum of 281 mb at 15.3 MeV. The $(\gamma, 2n)$ cross section rises to a maximum of 100 mb at 17.9 MeV. The $(\gamma, 3n)$ cross section rises to approximately 20 mb in the energy range from threshold (24.9 MeV) to 30 MeV. The singles data [Fig. 12(a)] show some structure on the high-energy side of the giant resonance, at about 23 MeV, and a sharp rise near the (γ, n) threshold, at approximately 9.5 MeV.

6. Sn^{124}. The data for Sn^{124} are given in Figs. 13(a)–13(d). The cross section rises to a peak value of 290 mb at 14.8 MeV. The $(\gamma, 2n)$ cross section has a peak value of 115 mb at 16.8 MeV, while the $(\gamma, 3n)$ cross section

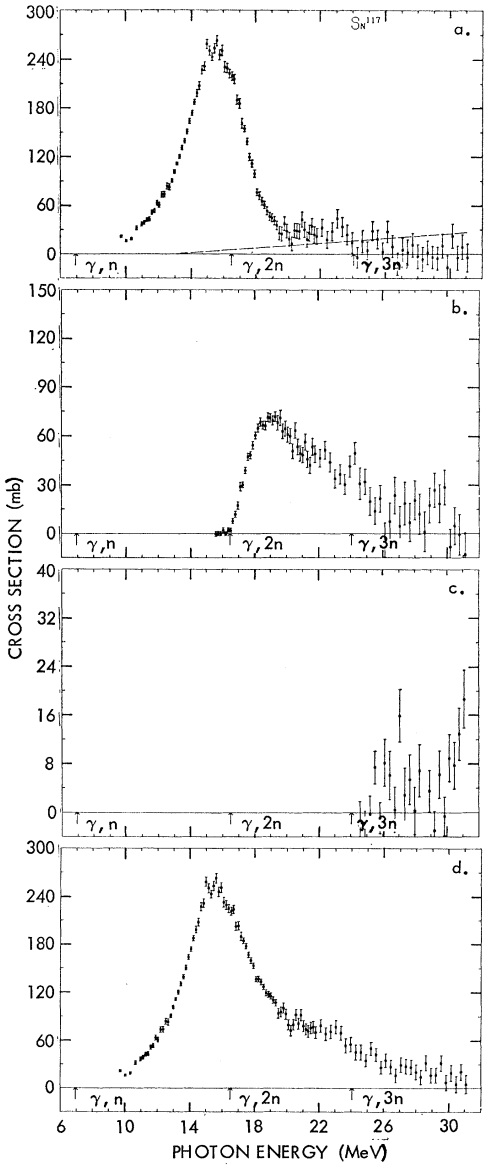

FIG. 11. (a) Single-photoneutron cross-section data $\sigma[(\gamma, n)+(\gamma, pn)]$ for γ rays incident on Sn^{119}. The dashed line represents the maximum increase in cross section which could be caused by a 4% uncertainty in the normalization constant. (b) Double-photoneutron cross-section data $\sigma(\gamma, 2n)$. (c) Triple-photoneutron cross-section data $\sigma(\gamma, 3n)$. (d) The total-photoneutron cross section $\sigma[(\gamma, n)+(\gamma, pn)+(\gamma, 2n)+(\gamma, 3n)]$. The data curve (d) can be fitted with a Lorentz line (up to 17 MeV) having parameters given in Table IV.

rises to 20 mb in the energy range from threshold (23.24 MeV) to 30 MeV. The cross section appears to rise sharply at the (γ, n) threshold and, as in the other cases, appears to show some structure on the high-energy side of the giant resonance.

7. *In*^{115}. The cross-section data for In^{115} are given in Figs. 14(a)–14(d). The cross section rises slowly from the (γ, n) threshold, unlike Sn^{124} and Sn^{120}, and shows only a little structure on the high side of the giant resonance in the region from 22 to 24 MeV. It reaches a maximum of 265 mb at 15.6 MeV. The $(\gamma, 2n)$ cross section has a peak value of 67 mb at 20.0 MeV. The $(\gamma, 3n)$ cross section is small but nonzero at 30 MeV.

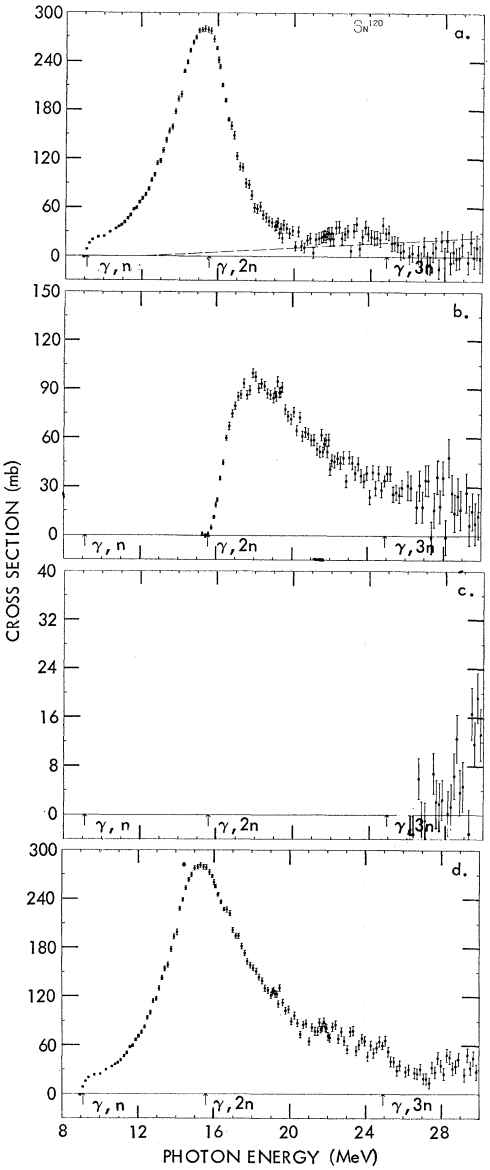

FIG. 12. (a) Single-photoneutron cross section $\sigma[(\gamma, n)+(\gamma, pn)]$ for γ rays incident on Sn^{120}. The dashed line represents the maximum increase in cross section which could be caused by a 4% uncertainty in the normalization constant. (b) Double-photoneutron cross section $\sigma(\gamma, 2n)$. (c) Triple-photoneutron cross section $\sigma(\gamma, 3n)$. (d) The total-photoneutron cross section $\sigma[(\gamma, n)+(\gamma, pn)+(\gamma, 2n)+(\gamma, 3n)]$. The data of (d) can be fitted with a Lorentz line (up to 17 MeV) with parameters given in Table IV.

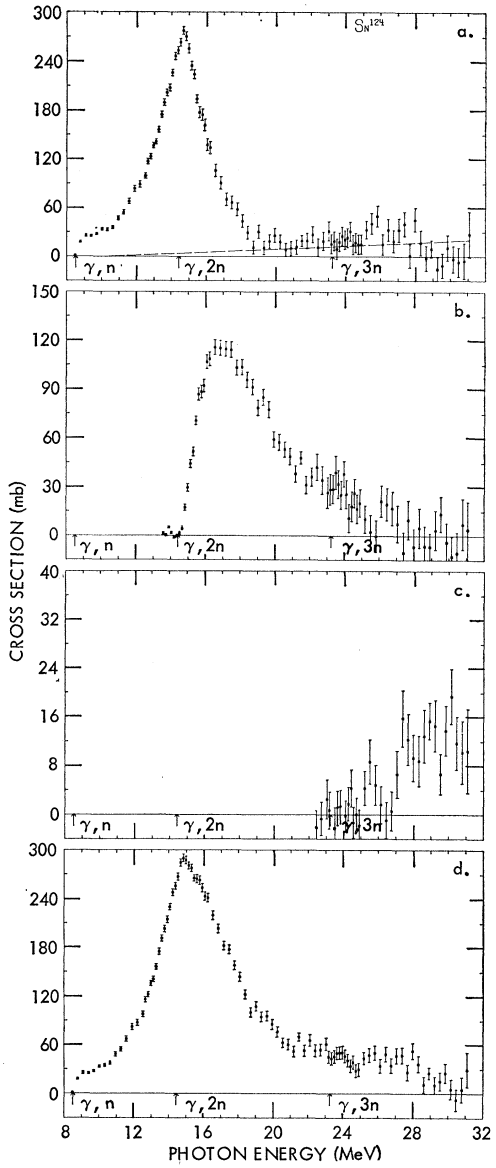

FIG. 13. (a) Single-photoneutron cross-section data $\sigma[(\gamma, n)+(\gamma, pn)]$ for γ rays incident on Sn^{124}. The dashed line represents the maximum increase in cross section which could be caused by a 4% uncertainty in the normalization constant. (b) Double-photoneutron cross section $\sigma(\gamma, 2n)$. (c) Triple-photoneutron cross section $\sigma(\gamma, 3n)$. (d) The total-photoneutron cross section $\sigma[(\gamma, n)+(\gamma, pn)+(\gamma, 2n)+(\gamma, 3n)]$. The data of (d) can be fitted with a Lorentz line (up to 17 MeV) with parameters given in Table IV.

III. DISCUSSION

A. Giant-Resonance Parameters

The giant-resonance parameters obtained from the fitting of Lorentz curves to the data are given in Table

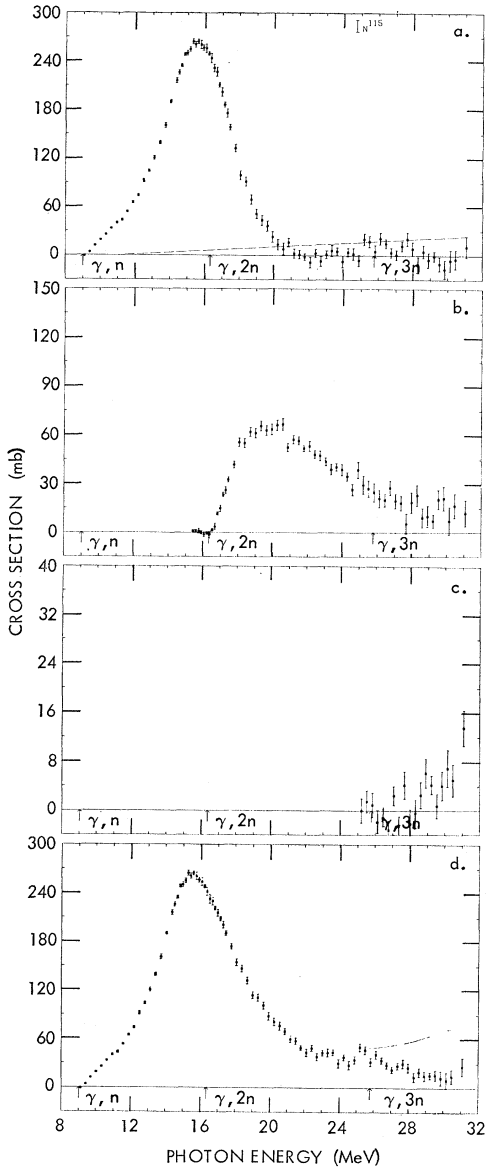

FIG. 14. (a) Single-photoneutron cross-section data $\sigma[(\gamma, n)+(\gamma, pn)]$ for γ rays incident on In^{115}. The dashed line represents the maximum increase in cross section which would be caused by a 4% uncertainty in the normalization constant. (b) Double-photoneutron cross section $\sigma(\gamma, 2n)$ for In^{115}. (c) Triple-photoneutron cross section $\sigma(\gamma, 3n)$ for In^{115}. (d) The total-photoneutron cross section $\sigma[(\gamma, n)+(\gamma, pn)+(\gamma, 2n)+(\gamma, 3n)]$ for In^{115}. The data of (d) can be fitted with a Lorentz line (up to 17 MeV) with parameters given in Table IV.

IV. The agreement of the energy dependence of the peak of the giant resonance, E_m, with the $A^{1/3}$ (Ref. 17) and $A^{1/6}$ (Ref. 18) laws is shown in Table V. From the data on the tin isotopes and indium, it is apparent that either of these laws is equally valid, since the range of the mass numbers is too limited to accentuate systematic deviations. The variation of the width of the giant resonance with mass number, or neutron number, is immediately apparent in Table IV. The minimum width (4.19 MeV) is obtained in the case of Sn^{116}, and this increases to about 4.88 MeV for Sn^{120}. However, the width is clearly not a smooth function of additional valence neutrons since Sn^{117} appears to be exceptionally broad.

The nuclear-symmetry–energy parameter K can be computed from the energies for the cross-section maxima E_m, through the relation[19]

$$E_m=(\hbar k/A)\{(8KNZ/M)[1-(\Gamma/2E_m)^2]\}^{1/2}, \quad (2)$$

where $\hbar$, A, N, Z, K, and M are the Planck constant, the mass, neutron, and atomic numbers, the symmetry energy, and the nucleon mass, respectively. The constant k is an eigenvalue of the scalar Helmholtz equation for nuclear-charge density.

Values for K are shown in Table V as calculated for the present data using the above formula and $kR=2.082$. (For this relation, R has the value $1.2A^{1/3}$ F and is the nuclear radius.) It is evident that these show remarkable constancy, having an average value of 24.3, which may be compared with the value of 23.0 obtained from mass analysis.[20]

B. Integrated Cross Sections

The integrated cross sections obtained from the present data are given in Table VI. Column 2 gives the integrated values for the single-neutron cross sections $\sigma[\gamma n+\gamma, pn]$. Column 3 gives the integrated values for the double-neutron cross sections. The total integrated cross section (column 5) is obtained from integration of $\sigma[(\gamma, n)+(\gamma, 2n)+(\gamma, 3n)+(\gamma, pn)]$. It is evident that the total integrated cross sections are as great as, or slightly exceed, the values given by the saturation of the Thomas-Reich-Kuhn dipole sum rule (column 9), without the addition of the exchange-force term. The average of the excess integrated cross section over the

TABLE V. The relation between E_m and mass number A.

Nucleus	$E_mA^{1/3}$ (MeV)	$E_mA^{1/6}$ (MeV)	K (MeV)
Sn^{116}	76.5	34.6	24.1
Sn^{117}	76.6	34.6	24.4
Sn^{118}	76.5	34.5	24.4
Sn^{119}	76.4	34.5	24.4
Sn^{120}	76.0	34.2	24.2
Sn^{124}	75.7	33.9	24.2
In^{115}	76.0	34.4	24.1
Averages	76.2	34.4	24.3

[17] H. Steinwedel and J. H. D. Jensen, Z. Naturforsch **5a**, 413 (1950).
[18] M. Goldhaber and E. Teller, Phys. Rev. **74**, 1046 (1948).
[19] M. Danos, Nucl. Phys. **5**, 23 (1958).
[20] A. E. S. Green, Phys. Rev. **95**, 1006 (1954).

TABLE VI. Integrated cross sections.

Nucleus	$\sigma_{int}[(\gamma, n)+(\gamma, pn)]$ (MeV b)	$\sigma_{int}(\gamma, 2n)$ (MeV b)	$\sigma_{int}(\gamma, 3n)$ (MeV b)	σ_{int}(total)[a] (MeV b)	$E_{\gamma max}$ (MeV)	$\frac{\sigma_{int}[(\gamma, 2n)+(\gamma, 3n)]}{\sigma_{int}(\gamma, \text{total})}$[b]	$(\pi/2)\sigma_m\Gamma$ (MeV b)	$0.06NZ/A$ (MeV b)
Sn^{116}	1.253	0.414	...	1.667	29.4	0.248	1.75	1.71
Sn^{117}	1.416	0.475	0.049	1.939	31.1	0.270	2.00	1.72
Sn^{118}	1.323	0.531	0.044	1.898	30.0	0.302	1.91	1.73
Sn^{119}	1.400	0.598	0.080	2.078	31.1	0.326	1.91	1.74
Sn^{120}	1.397	0.673	0.020	0.092	29.9	0.337	2.15	1.75
Sn^{124}	1.340	0.670	0.068	2.077	31.1	0.355	2.14	1.79
In^{115}	1.354	0.059	0.026	1.901	31.1	0.281	2.19	1.69

[a] Uncertainties in integrated cross sections are ±7%.
[b] Uncertainties in this ratio are ±10%.

sum-rule values is approximately 10% and is consistent with previous monochromatic photon data.[21] Column 7 gives the ratios of the integrated $(\gamma, 2n)$ cross sections and higher multiplicities to the total integrated cross sections. Column 8 of Table VI gives the total areas under the Lorentz lines.

The integrated moments deduced from the present measurement are presented in Table VII. The integrated moment σ_{-1} (column 3) is predicted[22] to be proportional to $A^{4/3}$. Column 4 of Table VII gives the proportionality constant. It varies over a range of values 0.175–0.209, or over approximately a 17% spread. This, however, is in disagreement with the values of 0.30 and 0.36 given in Ref. 22. The integrated second moment of the cross section, σ_{-2}, has been shown by Migdal to be proportional to $A^{5/3}$. Deviations from the theoretical value can be seen in column 6 of Table VII.

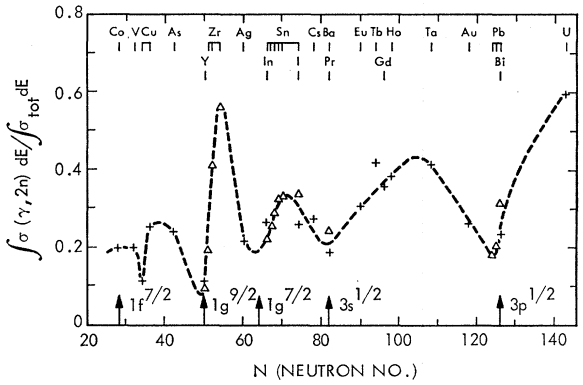

FIG. 15. Ratio of the integrated cross sections for $\sigma[(\gamma, 2n)+(\gamma, 3n)]/\sigma(\gamma, \text{tot})$ for the tin isotopes, and other isotopes measured at this Laboratory.

The second moment of the cross section is given by

$$\sigma_{-2}=\int_{E_{thr}}^{E_{max}}\sigma\frac{dE}{E^2}=\frac{\pi^2}{20}\frac{e^2}{hc}\frac{R^2A}{K}. \quad (3)$$

For $R=1.2A^{1/3}$ F, this reduces to $0.05175A^{5/3}K$ mb MeV^{-1} if K is in MeV. The values of K obtained from Eq. (3) are given in the last column of Table VII. It can be seen that they spread over a range of 16% from the calculated value of 23 MeV. The average value for the symmetry energy computed in this manner is 20.4 MeV.

C. Evidence for Nuclear-Shell Effects

As mentioned above, the data contained in column 7 of Table VI give the ratio of the integrated higher multiplicity to total cross sections for the isotopes discussed in the present report. It has been plotted in Fig. 15 along with similar data for other isotopes measured at this laboratory.[13–15,23–26] It has been plotted as a function of neutron number on the assumption that if shell effects are evident, they will occur in the neutron shells (rather than proton shells) for photoneutron processes. As can be seen in Fig. 15, marked minima occur in the vicinities of closed neutron shells and subshells.

For the zirconium and tin isotopes, the ratio increases as valence neutrons are added to closed-shell configurations. The isotopes Y^{89}, In^{115}, and Bi^{209} differ from Zr^{90}, Sn^{116}, and Pb^{208}, respectively, by one proton, yet have the same neutron number. If a neutron-shell effect were the dominating feature of the manner in which the ratio varies, similar values would be obtained despite the proton number. For the above isotopes this

[21] S. C. Fultz, R. L. Bramblett, B. L. Berman, J. T. Caldwell, and M. A. Kelly, in *Proceedings of the International Conference on Nuclear Physics, Gatlinberg, Tenn., 1966*, edited by R. L. Becker (Academic Press Inc., New York, 1967).
[22] J. Levinger, *Nuclear Photo-Disintegration* (Oxford University Press, New York, 1960).
[23] B. L. Berman, R. L. Bramblett, J. T. Caldwell, H. S. Davis, M. A. Kelly, and S. C. Fultz, Phys. Rev. **177**, 1745 (1969).
[24] R. L. Bramblett, J. T. Caldwell, B. L. Berman, R. R. Harvey, and S. C. Fultz, Phys. Rev. **148**, 1198 (1966).
[25] R. L. Bramblett, J. T. Caldwell, G. F. Auchampaugh, and S. C. Fultz, Phys. Rev. **129**, 2723 (1963).
[26] B. L. Berman, M. A. Kelly, R. L. Bramblett, J. T. Caldwell, H. S. Davis, and S. C. Fultz, University of California Radiation Laboratory Report No. UCRL-71747, 1968 (unpublished).

TABLE VII. Integrated moments of photoneutron cross sections and sum rules.

Nucleus	$E_{\gamma\max}$ (MeV)	σ_{-1} (mb)	$\sigma_{-1}A^{-4/3}$ (mb)	σ_{-2} (MeV^{-1} mb)	$\frac{\sigma_{-2}}{0.00225A^{5/3}}$	$\frac{\sigma_{-2}K}{0.05175A^{5/3}}$	$\frac{0.05175A^{5/3}}{\sigma_{-2}}$ (MeV)
Sn^{116}	29.4	94	0.175	6.13	0.987	1.027	23.3
Sn^{117}	31.1	114	0.199	7.30	1.157	1.229	19.9
Sn^{118}	30.8	110	0.189	6.85	1.070	1.131	21.5
Sn^{119}	31.1	119	0.203	7.55	1.166	1.235	19.7
Sn^{120}	29.9	124	0.209	7.78	1.186	1.245	19.4
Sn^{124}	31.1	123	0.200	8.02	1.158	1.219	19.7
In^{115}	31.1	113	0.209	7.13	1.166	1.223	19.7

is seen to be the case. Even more illustrative of this are the cases of Ba^{138} and Pr^{141}, which differ by three protons but have 82 neutrons, thus occurring at a neutron closed shell. It is seen that the ratios of the integrated values for the higher multiplicity to total cross sections for these isotopes are in good agreement and occur at a minimum on the curve.

The cases of Sn^{124} and I^{127}, which also differ by three protons, show agreement similar to Ba^{138} and Pr^{141}. That of Sn^{124} is particularly significant. The ratio of the integrated higher multiplicity to total cross section increases linearly from Sn^{116} until Sn^{120} is reached, at which point it increases less rapidly. As the mass number is increased, valence neutrons are being added to the $1g^{7/2}$ closed subshell (58 neutrons)[27] near Sn^{116}, and the neutron configuration moves towards the $3s^{1/2}$ closed shell (82 neutrons), where the ratio would be expected to be minimum once again. If this is so, it must begin to decrease in the region of Sn^{124} once again. Such is seen to be true, and the ratio for Sn^{124} is in agreement with the value obtained for I^{127}, with which it differs by three protons. These factors all demonstrate further evidence for the neutron-shell interpretation of this ratio.

Marked minima are seen to occur in the regions of the $1g^{9/2}$, $3s^{1/2}$, and $3p^{1/2}$ closed neutron shells. As neutrons are added to the $1g^{9/2}$ closed shell (50 neutrons) of the zirconium isotopes, a dramatic increase in the ratio of the integrated higher multiplicity to total cross sections is evident. In a similar manner, the ratio increases as neutrons are added to the other closed-shell configurations. Some anomalies to the rule are also in evidence. The case of Cu^{63} is such a one. This isotope shows a very low ratio despite the fact that its neutron configuration is nowhere near a closed shell. However, such a ratio based purely on neutron-production cross sections, and which does not include the (γ, p) cross section, is not truly representative of what the actual higher multiplicity to total cross-section ratio should be for the lower-mass-number elements, where (γ, p) cross sections are important. An additional anomaly occurs near the $3p^{1/2}$ (126 neutrons) closed shell. Instead of the minimum of the ratio occurring at Pb^{208}, it appears to occur at Pb^{206} and increases as neutrons are added to the Pb^{206} configuration.

[27] P. F. A. Klinkenberg, Rev. Mod. Phys. 24, 63 (1952).

D. Nuclear Level Densities

From measurements on the $(\gamma, 2n)$ cross sections, it is possible to calculate nuclear-level-density parameters and pairing effects. The expression used is as follows:

$$\frac{\sigma(\gamma, 2n)(E)}{\sigma(\gamma, \text{total})(E)} = \int_0^{E_\gamma - E_{\text{thr}}(\gamma,2n)} \rho(U) E_n dE_n \Big/ \int_0^{E_\gamma - E_{\text{thr}}(\gamma,n) - \Delta} \rho(U) E_n dE_n, \quad (4)$$

where $U = E_\gamma - E_{\text{thr}}(\gamma, n) - E_n - \Delta$ denotes the excitation energy of the target-minus-one neutron nucleus, Δ is a correction to the residual-nucleus ground state from shell and pairing effects; ρ is the level density, and can be described by either of the following formulas:

$$\text{(a)} \quad \rho \propto U^{-2} \exp[2(aU)^{1/2}], \quad \text{(Ericson)} \quad (5)$$

$$\text{(b)} \quad \rho \propto \exp[2(aU)^{1/2}], \quad \text{(Weisskopf)} \quad (6)$$

where a is the level-density parameter. Using a computer to perform a parameter search, it is possible to apply Eqs. (5) and (6) to (4) and obtain values for a, ρ, and Δ. This was done for data on the isotopes studied here, and the results are given in Table VIII. Here, columns 2 and 3 contain level-density parameters calculated from Eq. (6) for the cases where (the pairing energy) $\Delta = 0$, and $\Delta \neq 0$, respectively. Columns 4 and 5 contain the results for level densities calculated by use of Eq. (5), for the same cases. Columns 6 and 7 give values for the shell-plus-pairing effect, when either the Weisskopf or the Ericson formulas are used for the level density. A significant feature of Table VIII is the good agreement between values obtained for Δ regardless of the formula used to calculate the level density. In

TABLE VIII. Nuclear level densities and pairing energies.

Nucleus	Weisskopf a (MeV^{-1}) $\Delta=0$	Weisskopf a (MeV^{-1}) $\Delta\neq0$	Ericson a (MeV^{-1}) $\Delta=0$	Ericson a (MeV^{-1}) $\Delta\neq0$	Weisskopf Δ (MeV)	Ericson Δ (MeV)
Sn^{115}	8.1	4.5	13.1	10.3	3.0±0.5	2.7±0.4
Sn^{116}	7.3	2.7	11.4	8.3	5.8±0.8	5.0±0.8
Sn^{117}	5.6	2.6	10.2	8.2	3.0±0.5	2.7±0.4
Sn^{118}	13.2	6.7	18.4	10.5	5.0±0.7	5.0±0.7
Sn^{119}	3.6	1.5	7.8	6.1	3.2±0.5	2.6±0.4
Sn^{123}	5.4	3.3	10.2	8.8	2.0±0.3	1.9±0.3
In^{114}	4.6	2.5	8.6	7.0	3.0±0.4	2.9±0.4

addition, it is evident that values of Δ obtained for Sn^{117} and Sn^{119} are significantly higher than the others. Since Δ is a correction to the ground state of the residual nuclei, this applies to Sn^{116} and Sn^{118}, respectively, both of which are even-even nuclei. A similar effect was observed for the zirconium isotopes,[15] for which the value of Δ for Zr^{90} was significantly higher than the others.

E. Structure above the Giant Resonance

It has been noted that for most of the tin isotopes some structure has appeared on the high-energy side of the giant resonance. This structure might arise from one or several possible sources. Among these are (a) quadrupole contributions to the giant resonance and (b) additional dipole contributions decaying significantly through the (γ, pn) reaction channel, which might result from an analog giant resonance having isobaric spin one unit larger than the isobaric spin of the ground- and giant-resonance states. The latter has been proposed by Fallieros[28] and others. The approximate separation of this energy from the main giant-resonance-peak energy ΔE can be calculated for each isotope from the expression

$$\Delta E=\tfrac{1}{2}(100/A)[(T+1)(T+2)-T(T+1)-2], \quad (7)$$

where A is the atomic mass, and T is the isobaric spin of the ground state.

Quadrupole contributions to the photon-absorption cross section have been calculated by a number of authors.[29–32] The maximum of the $E2$ cross section, according to Lushniknov,[31] occurs at an energy given by

$$E_Q=190A^{-1/3}\ \text{MeV}. \quad (8a)$$

Danos, Griener, and Kohr have also derived an expression for the energy of the peak quadrupole cross section.[32] They obtain

$$E_Q=125A^{-1/3}\ \text{MeV}. \quad (8b)$$

The width at half-maximum, Γ, is given, approximately, by[31]

$$\Gamma=20A^{-1/3}\ \text{MeV}. \quad (9)$$

To interpret the structure on the high-energy side of the giant resonance, it is first necessary to compare the data with the results of calculations which have included most of the known factors likely to contribute to the structure. The treatment by Huber *et al.*[33] includes coupling between the dipole and quadrupole nuclear vibrations and was used to calculate the shape of the giant resonance for several of the tin isotopes.[34] The expression developed by these authors is

$$\sigma_a(E)=0.038(1+\alpha)(NZ/A)\sum_k (E_k q_k^2/E_1\Gamma_k) \times\{[(E^2-E_k^2)/E\Gamma_k]^2+1\}^{-1}, \quad (10)$$

where E_k, q_k^2, and Γ_k denote the energy, dipole strength, and width, respectively, of the component Lorentz lines; N, Z, and A are the neutron, atomic, and mass numbers, respectively; α is an enhancement factor to describe the effective mass; and E_1 is the energy of the giant dipole resonance.

The results of such calculations for Sn^{118} and Sn^{124} are shown in Figs. 16(a) and 16(b), respectively. For these calculations the height of the curve was normalized to the measured peak cross section, while the width Γ was obtained by matching the curve to the data in the energy region near the peak, i.e., 12–18 MeV. Contributions from the satellite dipole terms to the cross section beyond the region of matching would be expected. It is evident, however, that such contributions are in-

[28] S. Fallieros, B. Goulard, and R. H. Venter, Phys. Letters **19**, 398 (1965).
[29] V. G. Shevchenko, N. P. Yudin, and B. A. Yur'ev, Zh. Eksperim. i Teor. Fiz. (1963) [English transl.: Soviet Phys.—JETP **18**, 128 (1964)].
[30] Yu K. Khokhlov, Zh. Eksperim. i Teor. Fiz. **32**, 124 (1957) [English transl.: Soviet Phys.—JETP **5**, 88 (1957)].
[31] A. Lushnikov and M. Urin, Yadern. Fiz. **3**, 436 (1965) [English transl.: Soviet J. Nucl. Phys. **1**, 311 (1965)].
[32] M. Danos, W. Greiner, and B. C. Kohr, University of Freiburg Report, 1964 (unpublished).
[33] M. G. Huber, M. Danos, H. J. Weber, and W. Greiner, Phys. Rev. **155**, 1073 (1967).
[34] We are indebted to Dr. Hartmuth Arenhovel and Dr. W. Greiner for calculations on the dipole strengths and energies of Sn^{118}, Sn^{120}, and Sn^{124}.

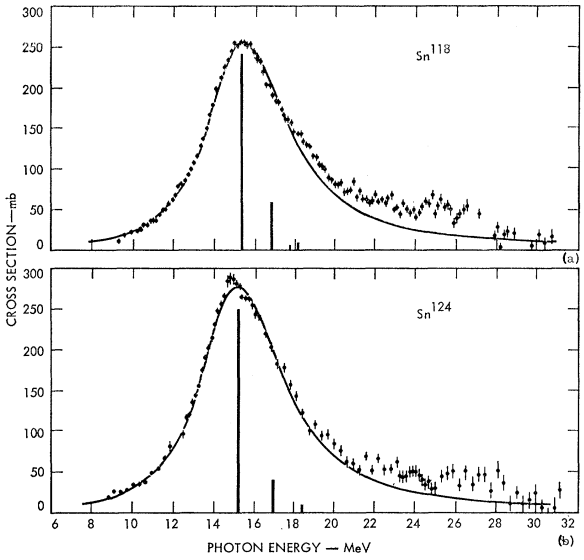

FIG. 16. Total-photoneutron cross-section data (16a) for Sn^{118} and (16b) for Sn^{124}, fitted with curves calculated from the theory of Huber *et al.* (Ref. 33). The vertical bars represent the relative dipole strength of the component Lorentz lines.

adequate to explain the structure on the high-energy side of the giant resonance.

The amount of cross section in excess of the calculated curves for Sn^{118} and Sn^{124} are shown in the graphs of Figs. 17(a) and 17(b), respectively. The solid vertical lines on the left denote the positions of the peaks of the giant resonances, while arrows marked Q and $T+1$ denote, respectively, the positions of the maxima of the contributions of the quadrupole and the $(T+1)$ isobaric states.

A summary of the properties of the quadrupole contributions to the giant resonances of the even-mass tin isotopes is given in Table IX. Columns 2 and 3 give the relative quadrupole integrated cross section and the energy, respectively, at the maxima, as deduced from the formulas of Lushnikov, while columns 5 and 6 give these same quantities deduced from the formulas of Danos and Greiner.[32] Column 7 contains values of Γ calculated by Eq. (8), while the peak cross sections of the column 8 are calculated from the expression

$$\sigma_{\max}(Q)=\frac{2}{\pi\Gamma}\frac{\sigma_{\text{quad}}(\text{int})}{\sigma_{\text{dip}}(\text{int})}\times\sigma_{\text{tot}}(\text{int}). \qquad (11)$$

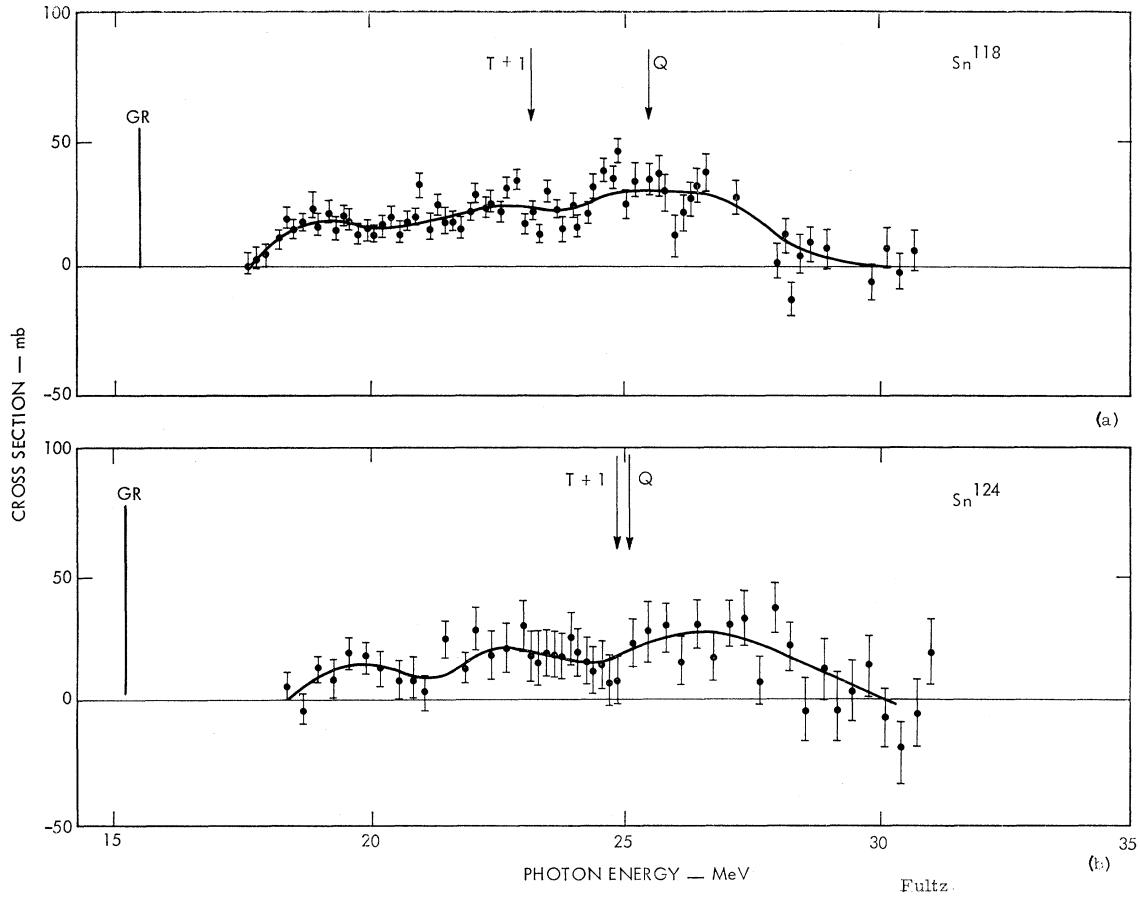

FIG. 17. (a) Excess cross section on the high-energy side of the giant resonance of Sn^{118} after subtraction of the theoretical component. (b) Excess cross section on the high-energy side of the giant resonance of Sn^{124} after subtraction of the theoretical component.

TABLE IX. Quadrupole contributions to the photon-absorption cross section.

Nuclei	Lushnikov[a] $\sigma_{quad}/\sigma_{dip}$	Lushnikov[a] $E_m=190/A^{1/3}$ (MeV)	Danos *et al.*[b] $\sigma_{quad}/\sigma_{dip}$	Danos *et al.*[b] $E_m=125/A^{1/3}$ (MeV)	Experimental $\sigma_{quad}/\sigma_{dip}$	Quadrupole Γ (MeV)	Quadrupole σ_{max} (mb)
Sn^{116}	0.19	39.0	0.08	25.6	0.111	4.10	29
Sn^{118}	0.18	38.7	0.08	25.5	0.123	4.08	36
Sn^{120}	0.18	38.5	0.08	25.3	0.125	4.06	41
Sn^{124}	0.18	38.1	0.08	25.1	0.085	4.02	26

[a] From Ref. 31.
[b] From Ref. 32.

Identical plots and analyses were made for Sn^{116} and Sn^{120}. The plots were similar to those for Sn^{118} and Sn^{124}, and the results are also shown in Table IX.

It is evident from these data and from Fig. 17 that much of the excess cross section observed for the isotopes Sn^{118} and Sn^{124} can be described in terms of quadrupole contributions to the giant resonance, since the expected width is broad. This is in contrast to the expected width of the $(T+1)$ analog states, which are only a few hundred kilovolts. Such an argument does not, however, rule out the possibility that contributions from analog states are present in the structure on the high-energy side of the giant resonance, since there could be several of them.

On the high-energy side of the giant resonance, in some cases at least, the (γ, pn) reaction might be the mode of decay. In the cases of Sn^{117}, Sn^{118}, Sn^{120}, Sn^{124}, and In^{115}, this is particularly suggestive, as can be seen from the singles cross-section curves 9(a), 10(a), 12(a), 13(a), and 14(a), respectively. In these cases, the (γ, pn) thresholds occur towards the high-energy limit of the giant resonances, and contributions from the (γ, pn) reaction, therefore, should rise to a maximum beyond the main portion of the giant resonance for the total cross section. The (γ, pn) reaction is not forbidden by isobaric-spin selection rules and could arise from excitation to $T+1$ states, as well as from ordinary dipole excitation.

F. Comparison with Previous Measurements

For the 17.1-MeV Li(p, γ) photons, the value of the natural tin cross section [obtained from Figs. 8(c), and 9(d)–13(d), after multiplying by the relative abundance] is 186±13 mb. This appears to be in good agreement with the value 195 mb obtained by Hartley *et al.*[2] For the natural tin peak cross section, a value of approximately 270±17 mb is obtained. This may be compared with the previous values of 300, 340±40, and 300±30 listed in Table I for the "yield cross section" $\sigma[(\gamma, n)+(\gamma, pn)+2(\gamma, 2n)+3(\gamma, 3n)]$. The latter are obviously too high, even though multiplicity corrections would be small at the peak of the giant resonance (at approximately 15.5 MeV). The calculated value for the integrated cross section for natural tin, obtained from Table VI, is 1990±140 MeV mb. This exceeds the values 1830 and 1860 given in Table I for the yield cross section. The value 1560±80 MeV mb for the yield cross section of Sn^{124} given in Table I is considerably below that of 2077±140 MeV mb given in Table VI, where multiplicity corrections have been included.

The data on indium obtained in the present experiment give total photoneutron cross sections of 35±3 and 13±2 mb at 10.8 and 9.7 MeV, respectively. These may be compared favorably with the values of 33.3±2.7 and 17.1±2.6 obtained with monochromatic γ rays by Hurst and Donahue.[9] The peak cross section of 266±7 mb agrees with the value 280±29 obtained by Bogdankevich.[8] The integrated total cross section for indium, 190±133 MeV mb (from Table VI), also agrees reasonably well with the value 1800 MeV mb listed in Table I.

IV. SUMMARY AND CONCLUSIONS

The cross sections for the (γ, n), $(\gamma, 2n)$, and $(\gamma, 3n)$ reactions have been measured for the tin isotopes Sn^{116}, Sn^{117}, Sn^{118}, Sn^{119}, Sn^{120}, and Sn^{124} and for indium. Integrated cross sections, integrated moments, giant resonance, and statistical parameters have been deduced from the cross-section data. Where possible, these have been compared with theory: (1) Integrated cross sections are, on the average, about 10% above those deduced from the dipole sum rule, with no addition of an exchange-force term to the latter. (2) Widths of the giant resonances exhibit a gradual increase with mass number, with the exception of Sn^{117}. (3) The shell-and pairing energies, when calculated with either the Weisskopf or Ericson level-density formula are in good agreement with each other. They show a marked increase when the residual nucleus is even-even. (4) There is considerable evidence of structure in the cross section for the energy region above the giant resonance. This structure may be attributed to a number of factors, including quadrupole excitation, $(T+1)$ isobaric states or dipole excitation. The (γ, pn) reaction is a likely mode of decay for excitation in this region. (5) The higher-multiplicity–to–total-integrated-

cross-section ratio shows a strong dependence on neutron-shell configuration. It exhibits minima at closed shells or subshells and increases markedly as the number of valence neutrons are added to the closed-shell configurations. (6) The data of the present experiment agree well with previous measurements obtained by the use of monochromatic photons.

ACKNOWLEDGMENTS

The authors would like to express their appreciation to E. Dante and the Linac operators for their cooperation during the experiments, to Miss C. Hunt for her assistance with computer codes, and to Dr. H. S. Davis for help during the experiment.

PHYSICAL REVIEW VOLUME 186, NUMBER 4 20 OCTOBER 1969

Level Structure of $Te^{116, 118, 120, 122}$ †

E. H. SPEJEWSKI, P. K. HOPKE,* AND F. W. LOESER, JR.

Palmer Physical Laboratory, Frick Chemical Laboratory, and Princeton-Pennsylvania Accelerator, Princeton University, Princeton, New Jersey 08540

(Received 26 May 1969)

The decays of $I^{116,118,120,122}$ have been studied by use of isotopically separated sources produced by proton spallation of lanthanum. Ge(Li) γ-ray singles spectra and Ge(Li)-Ge(Li) coincidence spectra have been obtained and used in constructing level schemes for the corresponding Te daughters.

I. INTRODUCTION

THE study of the neutron-deficient, even-even Te isotopes was undertaken because these nuclides appeared to offer a good opportunity to study collective effects in the spherical region. The Te nuclei lie just above the closed proton shell at 50 and are expected to be quite "spherical." However, because the proton shell is not closed, it is expected that the first $E2$ excitation should lie considerably lower than those in the tin isotopes and should, therefore, be well separated from single-particle states at higher energies. It was hoped that a study of the level structure of these nuclei might yield some information about the nature of the collective states in this region. In particular, it was anticipated that the characteristics of these even collective levels might conform to the expectations of the quadrupole-vibrational model. Although rather generally considered insufficient, this model should correspond quite closely to the structure of the Te nuclei if it has any validity at all.

The first reported work on the neutron-deficient Te nuclei was performed by Andersson *et al.*[1] who obtained half-lives and Q-values for the β decays of I^{118} and I^{120}. They also reported some γ-ray transitions observed with a NaI spectrometer. Similar work was later reported by Butement and Qaim,[2] who also studied the decay of I^{122}.

When our investigation commenced, the knowledge of the level structure of Te^{118} and Te^{120} was very incomplete; only the approximate positions of the first excited states were known with any degree of certainty. During the course of our work, the results of Bergström, *et al.*[3] were communicated to us. These authors studied the levels in even-even Te nuclei by means of the $(\alpha, 2n)$ reaction and reported, in general, a 2^+ state at about 550–600 keV, a 2^+–4^+ doublet at about 1200 keV and a 6^+ state at about 1800 keV. These results are in quite good agreement with our preliminary results.[4]

While our final results were being correlated, those of the interesting experiments by Ladenbauer-Bellis and Bakhru[5] were published. They reported the existence of isomers in I^{118} and I^{120} and studied the decays of these isomers as well as those of the ground states. In addition to the levels already reported, they also placed a doublet at about 2100 keV in Te^{120}. One further, apparently preliminary, report[6] has also recently appeared.

II. EXPERIMENTAL PROCEDURE

A. Source Preparation

The isotopes of interest were formed by means of high-energy spallation reactions. La foils (approximately $38\times16\times0.25$ mm) were bombarded with 3-GeV protons from the Princeton-Pennsylvania Accelerator for nominal 1-h periods. In order to provide a large target thickness while minimizing the total amount of

† Work supported by the U.S. Atomic Energy Commission.

* Atomic Energy Commission Special Fellow in Nuclear Science and Engineering; Present address: Chemistry Dept., Massachusetts Institute of Technology, Cambridge, Mass.

[1] G. Andersson, G. Rudstam, and G. Sörensen, Arkiv Fysik **28**, 37 (1964).

[2] F. D. S. Butement and S. M. Qaim, J. Inorg. Nucl. Chem. **27**, 907 (1965); **27**, 1729 (1965).

[3] I. Bergström, C. J. Herrlander, A. Kerek, and A. Luuko (private communication).

[4] E. H. Spejewski, Bull. Am. Phys. Soc. **13**, 624 (1968).

[5] I.-M. Ladenbauer-Bellis and H. Bakhru, Phys. Rev. **175**, 1507 (1968).

[6] R. A. Warner and J. E. Draper, Bull. Am. Phys. Soc. **14**, 490 (1969).